Cluster as a wave telescope? first results from the fluxgate magnetometer

Karl-Heinz Glassmeier, U. Motschmann, M. Dunlop, A. Balogh, M. H. Acuña, C. Carr, G. Musmann, K.-H. Fornaçon, K. Schweda, J. Vogt, et al.

Annales Geophysicae (2001) 19: 1439–1447 © European Geophysical Society 2001

Annales Geophysicae

Cluster as a wave telescope – first results from the fluxgate magnetometer

K.-H. Glassmeier[1], U. Motschmann[2], M. Dunlop[3], A. Balogh[3], M. H. Acuña[4], C. Carr[3], G. Musmann[1], K.-H. Fornacon[1], K. Schweda[1], J. Vogt[1], E. Georgescu[5], and S. Buchert[6]

[1]Institut für Geophysik und Meteorologie, Technische Universität Braunschweig, Germany
[2]Institut für Theoretische Physik, Technische Universität Braunschweig, Germany
[3]Space and Atmospheric Physics Group, Imperial College, London, United Kingdom
[4]Goddard Space Flight Center, Greenbelt, USA
[5]Max-Planck-Institut für extraterrestrische Physik, Garching, München, Germany
[6]Swedisch Space Research Institute, Uppsala, Sweden

Received: 19 March 2001 – Revised: 22 June 2001 – Accepted: 23 June 2001

Abstract. The four Cluster spacecraft provide an excellent opportunity to study spatial structures in the magnetosphere and adjacent regions. Propagating waves are amongst the interesting structures and for the first time, Cluster will allow one to measure the wave vector of low-frequency fluctuations in a space plasma. Based on a generalized minimum variance analysis wave vector estimates will be determined in the terrestrial magnetosheath and the near-Earth solar wind. The virtue and weakness of the wave telescope technique used is discussed in detail.

Key words. Electromagnetics (wave propagation) – Magnetospheric physics (MHD waves and instabilities; plasma waves and instabilities)

1 Introduction

Cluster is more than just a four spacecraft mission, Cluster is an entirely new tool in space science which combines measurements from four different spacecraft to allow one to determine spatial variations with respect to temporal variations. Several new multi-spacecraft instruments can be built by correlating observations from the different spacecraft. These new instruments are, for example, the *curlometer* and the *discontinuity analyzer* (e.g. Dunlop et al., 1988, 1997, 1999) as well as the *wave telescope* (e.g. Musmann et al., 1974; Neubauer and Glassmeier, 1990; Pinçon and Lefeuvre, 1991, 1992; Stein et al., 1993; Glassmeier et al., 1995, Motschmann et al., 1995, 1996; Pinçon and Motschmann, 1998), which has its roots in array signal analysis techniques developed for the interpretation of seismic array data (e.g. Capon et al., 1967; Harjes and Henger, 1973).

Correspondence to: K.-H. Glassmeier
(kh.glassmeier@tu-bs.de)

In this paper, we shall outline, in particular, the wave telescope technique as described by Motschmann et al. (1996) and apply the wave telescope for the first time to real measurements in space received from the fluxgate magnetometers operated on board the Cluster spacecraft. These magnetic field instruments allow one to measure the magnetic field vector at a precision up to 8 pT at a temporal resolution up to 67 Hz. For further details of the Cluster fluxgate magnetometers, the reader is referred to Balogh et al. (1997).

The present study aims at testing the new analysis tool by applying it to magnetometer measurements in the magnetosheath, as well as the near-Earth solar wind plasma. It is our aim to demonstrate the feasibility of the wave telescope and its applicability in studying wave properties, in particular, the wave length and $\boldsymbol{k}$-vectors, as well as the wave propagation direction. First, we shall outline the theoretical foundations of the method and apply it to artificial data to demonstrate the usefulness of this tool. Using the results from the artificial data we shall also introduce several ways of graphically displaying the results. Second, we shall apply the new tool to compressional magnetic field fluctuations in the magnetosheath and discuss the results. Finally, small amplitude transverse fluctuations in the near-Earth solar wind will be analyzed.

The data we shall use are spin-averaged data with a time resolution of 4 s. The data are represented in the GSE-coordinate system, which will also be the frame of reference for all other vector quantities used. We either give full vectors in rectangular coordinates or the longitude and latitude in the associated spherical coordinate system.

2 Theory and practice of the wave telescope

The wave telescope represents a generalized minimum variance technique applied to multi-station measurements in or-

der to determine both wave vectors, as well as their associated wave power. Any magnetic field vector $\boldsymbol{b}(\omega, \boldsymbol{r}_{s/c})$ measured at the four Cluster spacecraft is represented as a series of plane propagating waves,

$$\boldsymbol{b}(\omega, \boldsymbol{r}_{s/c}) \;=\; \sum_{n=1}^{N} \boldsymbol{b}(\omega, \boldsymbol{k}_n) \cdot \exp(i\boldsymbol{k}_n \cdot \boldsymbol{r}_{s/c}), \tag{1}$$

where ω denotes the wave angular frequency, N is the number of plane waves composing the measured signal, and $\boldsymbol{k}_n$ is the corresponding wave vector. Equation (1) already defines the problem to be solved: given the measurements $\boldsymbol{b}(\omega, \boldsymbol{r}_{s/c})$, one must determine the weight or polarization vector $\boldsymbol{b}(\omega, \boldsymbol{k}_n)$ of each member of the wave ensemble that constitutes the wave. Thus, the wave telescope described and used here is essentially a wave decomposition technique. Here, plane propagating waves are used as a set of basis functions for the decomposition. Of course, the method outlined can also be formulated using spherical waves or any other useful system of elementary waves.

The measurements may be combined into the column vector

$$\boldsymbol{B}(\omega) \;=\; \left[\boldsymbol{b}(\omega, \boldsymbol{r}_1), \boldsymbol{b}(\omega, \boldsymbol{r}_2), \boldsymbol{b}(\omega, \boldsymbol{r}_3), \boldsymbol{b}(\omega, \boldsymbol{r}_4)\right]^T, \tag{2}$$

where the superscript "T" denotes the transposed vector. With the propagation matrix (caligraphic symbols denote tensor quantities)

$$\mathcal{H}(\boldsymbol{k}_n) \;=\; \left[\mathcal{I}e^{i\boldsymbol{k}_n\cdot\boldsymbol{r}_1}, \mathcal{I}e^{i\boldsymbol{k}_n\cdot\boldsymbol{r}_2}, \mathcal{I}e^{i\boldsymbol{k}_n\cdot\boldsymbol{r}_3}, \mathcal{I}e^{i\boldsymbol{k}_n\cdot\boldsymbol{r}_4}\right] \tag{3}$$

we have

$$\boldsymbol{B}(\omega) \;=\; \sum_{n=1}^{N} \mathcal{H}(\boldsymbol{k}_n)\boldsymbol{b}(\omega, \boldsymbol{k}_n). \tag{4}$$

Now, a covariance matrix containing all the measured data is defined as the expectation

$$\mathcal{M}_B(\omega) \;=\; E\left[\boldsymbol{B}(\omega)\boldsymbol{B}^{+}(\omega)\right], \tag{5}$$

where the superscript "+" denotes the Hermitian adjoint. The covariance matrix of the desired weight vectors is defined by the expectation

$$\mathcal{P}_b(\omega, \boldsymbol{k}_n) \;=\; E\left[\boldsymbol{b}(\omega, \boldsymbol{k}_n)\boldsymbol{b}^{+}(\omega, \boldsymbol{k}_n)\right]. \tag{6}$$

Both covariance matrices are related via the propagation matrix:

$$\mathcal{M}_B \;=\; \sum_{n=1}^{N} \mathcal{H}(\boldsymbol{k}_n)\mathcal{P}_b(\omega, \boldsymbol{k}_n)\mathcal{H}^{+}(\boldsymbol{k}_n). \tag{7}$$

The task is to find the best estimator for $\mathcal{P}_b(\omega, \boldsymbol{k}_n)$, which requires one to scan the entire $\boldsymbol{k}$-space and to find a suitable decomposition of the measured wave field. This involves the construction of an appropriate filter or projection procedure. Here, we require that our filter or projector matrix $\mathcal{W}(\boldsymbol{k})$ eliminates all signals that do not correspond to a given wave vector $\boldsymbol{k}$, i.e. one has

$$\mathcal{P}_b(\omega, \boldsymbol{k}_n) \;=\; \mathcal{W}^{+}(\boldsymbol{k}_n)\, \mathcal{M}_B\, \mathcal{W}(\boldsymbol{k}_n) \tag{8}$$

with the constraint

$$\mathcal{W}^{+}(\boldsymbol{k}_n)\, \mathcal{H}(\boldsymbol{k}_n) \;=\; \mathcal{I}. \tag{9}$$

According to Pinçon and Lefeuvre (1991) and Motschmann et al. (1996), a suitable projector matrix results from minimizing the trace of the covariance matrix $\mathcal{P}_b(\omega, \boldsymbol{k}_n)$ under the constraint (9). This yields a covariance matrix of the form (for details, see Motschmann et al., 1996):

$$\mathcal{P}_b(\omega, \boldsymbol{k}_n) \;=\; \left(\, \mathcal{H}^{+}(\boldsymbol{k}_n)\, \mathcal{M}_B^{-1}\, \mathcal{H}(\boldsymbol{k}_n)\, \right)^{-1}. \tag{10}$$

The trace of this cross-spectral density matrix gives the power associated with a specified plane wave and its contribution to the measured signal. Further refinements are possible, i.e. in addition to the filter condition (9), other conditions such as the solenoidality of the magnetic field or specifications with respect to the wave mode may be used to constrain the filter matrix $\mathcal{W}$. For further details, the reader is referred to Motschmann et al. (1996, 1998).

There are a couple of weak points or aspects which need to be addressed before using the tool outlined: plane wave assumption, stationarity and homogeneity requirement, spacecraft motion, and spatial aliasing.

In defining the propagation matrix, we made the assumption that the propagating wave fields are plane waves. This seems at first to be a major restriction, but actually it is not. Spherical waves, for example, may be expanded using plane waves as a basis to formulate the propagation matrix. This provides one with a complete representation of the measured wave field, similar to the way a frequency spectral analysis with time harmonic functions provides one with a complete representation of a time series. A plane wave assumption is mathematical fully justified, but may be physically awkward as the interpretation is complicated. If one knows a priori that the wave field consists of spherical waves, for example, then the propagation matrix should be formulated in terms of spherical waves. Here, we would like to mention that the wave telescope tool discussed does not rely on any assumptions such as wave dispersion properties.

Application of the above outlined method is based on the requirement of time stationary and space homogeneous conditions, i.e. the background magnetic field should neither exhibit major temporal trends nor large spatial gradients. We shall check for this condition by using a simple approach. We determine the mean magnetic field magnitude and direction, as well as the scattering of these parameters for the intervals analyzed. The statistics is done over time and the four spacecraft as the motion of the whole Cluster configuration mixes spatial and temporal variations. If the scattering of the magnitude and the direction of the mean-magnetic field is small, then we shall assume a data interval to represent a stationary and homogeneous situation. A more detailed analysis of the effect of any non-stationarities will be the subject of future work.

Motion of the four spacecraft is another effect which will influence the results. We determine the mean velocity of the four spacecraft and the distance they travel during the analysis interval. If this distance is small compared to the mean

distance between the spacecraft, then we assume that spacecraft motion does not effect the results obtained.

Spatial aliasing is a further effect to be taken into account and has been discussed in detail by Neubauer and Glassmeier (1990) (see also Pinçon and Motschmann, 1998; Chanteur, 1998). Using Laue's equations (e.g. Kittel, 1973) the spatial aliasing problem may be expressed as (e.g. Neubauer and Glassmeier, 1990)

$$\delta \boldsymbol{k} \cdot \boldsymbol{r}_n \;=\; 2\pi N_n; \quad n = 1, 2, 3, 4 \quad N \in \mathcal{N} \tag{11}$$

where the $\delta \boldsymbol{k}$ are generating vectors of the k-cell, i.e. the subvolume of the k-space closest to $\boldsymbol{k} = 0$, to which we restrict the $\boldsymbol{k}$-analysis to avoid spatial aliasing problems. The four vectors $\boldsymbol{r}_n$ are the position vectors of the four Cluster spacecraft. With the fundamental translations of the reciprocal spacecraft lattice, the three solutions of Laue's equations are given by

$$\delta \boldsymbol{k}_1 \;=\; \frac{2\pi}{V}\, \boldsymbol{r}_{31} \times \boldsymbol{r}_{21} \tag{12}$$

$$\delta \boldsymbol{k}_2 \;=\; \frac{2\pi}{V}\, \boldsymbol{r}_{41} \times \boldsymbol{r}_{21} \tag{13}$$

$$\delta \boldsymbol{k}_3 \;=\; \frac{2\pi}{V}\, \boldsymbol{r}_{41} \times \boldsymbol{r}_{31} \tag{14}$$

with

$$V \;=\; \boldsymbol{r}_{41} \cdot (\boldsymbol{r}_{31} \times \boldsymbol{r}_{21}), \tag{15}$$

where the $\boldsymbol{r}_{j1} = \boldsymbol{r}_j - \boldsymbol{r}_1, \quad j = 2, 3, 4$, are the distance vectors of the spacecraft 2, 3, and 4 with respect to spacecraft 1. Spatial aliasing does not occur if all the $\boldsymbol{k}$-vectors of the wave field lay inside the subvolume or k-cell, described by

$$\boldsymbol{k} \;=\; \sum_{n=1}^{3} \xi_n\, \delta \boldsymbol{k}_n; \quad -0.5 < \xi_n \leq 0.5. \tag{16}$$

As a less complex but more practical approach, we shall define a spatial Nyquist wave number

$$k_{NY} \;=\; \frac{\delta k_{min}}{2} \tag{17}$$

with δk_{min} as the minimum distance between opposing parallelogram sides of the parallelepiped constituting the k-cell. Wave vectors with wave numbers $k < k_{\mathrm{NY}}$ are part of the k-cell defined above and constitute a spatial Nyquist sphere imbedded in the k-cell. Thus, the spatial Nyquist wave number is a more conservative definition of the non-aliased part of the k-space. It will be used in the following applications of the wave telescope.

Changes in the relative distance of the spacecraft during an analysis interval may influence the aliasing properties of the spacecraft configuration used. Here, we assume that the aliasing properties are quasi-stationary as long as the change in relative distance is less than 5% of the minimum spacecraft distance.

The applicability of the above outlined wave analysis tool has been demonstrated by Motschmann et al. (1996) for the case of 2D wave propagation using artificial magnetic field data. To demonstrate the usefulness of the method in the 3D case, as well as its practical application, we have constructed an artificial set of Cluster measurements using actual observations of the Cluster 1 spacecraft made in the interval on 26 December 2000, 10:00–12:30 UT, when the spacecraft was in the terrestrial magnetosheath. These Cluster 1 measurements exhibit a turbulent type frequency spectral decay with a spectral index of about -2 and no pronounced spectral peak. They are thus a suitable background signal to which we have added a 20 mHz plane wave signal with the propagation vector $(-6.25 \cdot 10^{-4}, 2.5 \cdot 10^{-3}, -2.5 \cdot 10^{-3})$ km^{-1} and the polarization vector (10.0, -2.5, 2.5) nT. At each of the four spacecraft positions, the corresponding plane wave signal has been added. The chosen configuration of the four spacecraft was almost that of a tetrahedron with a mean distance to the center of 137 km and a maximum distance between two spacecraft of 543 km. The spacecraft are not moving in our simulated signals. The configuration was described by a configuration quality index $Q_{GM} = 2.8$, where Q_{GM} is defined as (Stein et al., 1992; Robert et al., 1998)

$$Q_{GM} \;=\; 1 + \frac{\text{True Surface}}{\text{Ideal Surface}} + \frac{\text{True Volume}}{\text{Ideal Volume}} \tag{18}$$

where "true" and "ideal" indicate the actual surface and volume of the configuration as compared to that of the regular tetrahedron.

The application of the wave telescope first requires the selection of a suitable wave frequency for which the analysis is done. A suitable choice may be any clear spectral peak of the data interval analyzed. Our artificial signal exhibits such a peak at 20 mHz, which has been selected as the analysis frequency.

There are, in principle, two ways to estimate the covariance matrix $\mathcal{P}_b(\omega, \boldsymbol{k}_n)$: either by averaging the spectral contributions in the frequency domain or by analysis of several consecutive time intervals and then subsequent averaging. Experimentally, we found that a better estimator was received when using time-averaging rather than frequency-averaging. Thus, we analyzed intervals of duration of 1024 data points, shifted by 64 data points 16 times. This implies that the overall time interval analyzed was 2048 data points long. In terms of a classical spectral analysis, 32 degrees of freedom are used in constructing the spatial spectrum. The Fourier analysis results from these 16 intervals are then used to construct the covariance matrix $\mathcal{M}_B(\omega) = \sum_{i=1}^{16} \mathcal{M}_{B,i}(\omega)$.

Once the frequency analysis has been performed, an appropriate part of the k-space must be scanned. This has been done in spherical coordinates with an angular resolution of 4°, i.e. 45 and 90 points in latitude and longitude, respectively, have been used. In the radial direction, i.e. in the wave number direction, 50 points have been used in the interval $(0, k_{\mathrm{NY}})$, where k_{NY} is the Nyquist wave number. The Nyquist wave length has been determined in the above described calculation; a value of 0.012 km^{-1} results

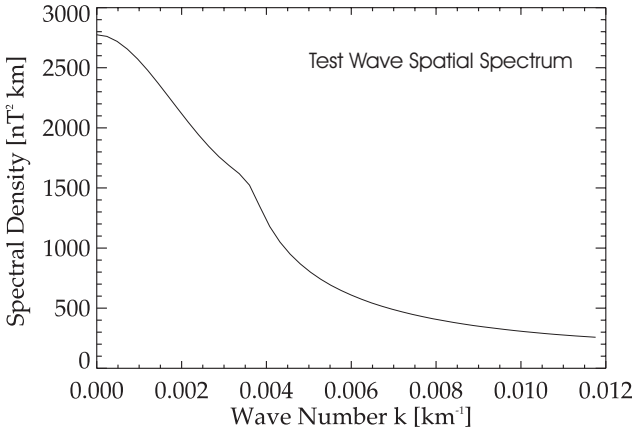

Fig. 1. Spatial spectral density distribution resulting from applying the wave telescope to the artificial data set.

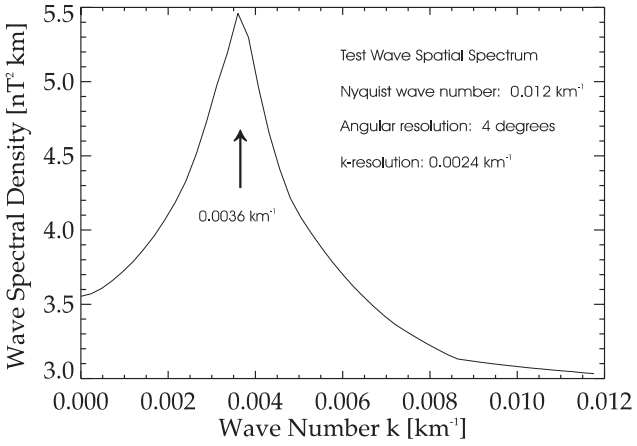

Fig. 2. Shell-max spatial spectral density distribution in logarithmic presentation resulting from applying the wave telescope to the artificial data set.

and the resolution in the wave number direction is thus given as $0.0024\,\mathrm{km}^{-1}$.

With these processing parameters, the k-space has been scanned and the trace $Tr\ \mathcal{P}_b(\omega, \boldsymbol{k}_n)$ was determined. Figure 1 displays the wave number spectral density spectrum, which has been derived by averaging $Tr\ \mathcal{P}_b(\omega, \boldsymbol{k}_n)$ over all latitudes and longitudes for a particular value of $|\boldsymbol{k}_n|$ and normalizing the resulting integrated power by (45×90), the number of $\boldsymbol{k}$-vectors associated with a prescribed value of $|\boldsymbol{k}_n|$. In the following, we shall denote the spectral density distribution derived in this way as the spatial spectral density. It has lost all resolution in direction, but provides a suitable representation of the power with respect to $|\boldsymbol{k}_n|$. It should be noted that this spectrum is very much influenced by the averaging procedure used. Even if there is a prominent spectral peak at a certain value of $\boldsymbol{k}_n$, this peak will be smeared out due to the averaging process. This can be seen in Fig. 1, where the general decaying nature of the spectral density with increasing $\boldsymbol{k}$ is perturbed by a slight increase at about $0.0036\,\mathrm{km}^{-1}$. To increase the visibility of this possible spectral enhancement, we introduce a new spectral density which we call shell-max wave spectral density. This shell-max spectral density is defined as the maximum spectral density of each given k-shell. Figure 2 shows such a shell-max spectrum density distribution or shell-max spectrum for our test wave. Now a clear spectral peak is visible at $0.0036\ \mathrm{km}^{-1}$, i.e. the k-value already indicated in Fig. 1, and corresponds to the dominant wave in our test data. For the k-shell corresponding to the peak value, Fig. 3 displays the power distribution as a function of longitude and latitude in a Mercator projection. A clear and well confined power peak appears at longitude 104° and latitude −46°, corresponding to a $\boldsymbol{k}$-vector $(-0.0006, 0.0024, -0.0026)\ \mathrm{km}^{-1}$. The main propagating wave found using the wave telescope is thus identical to the one used in constructing the artificial set of measurements. By increasing the resolution in the k-space, an even better agreement can be achieved, but this requires an increased amount of computation. We conclude

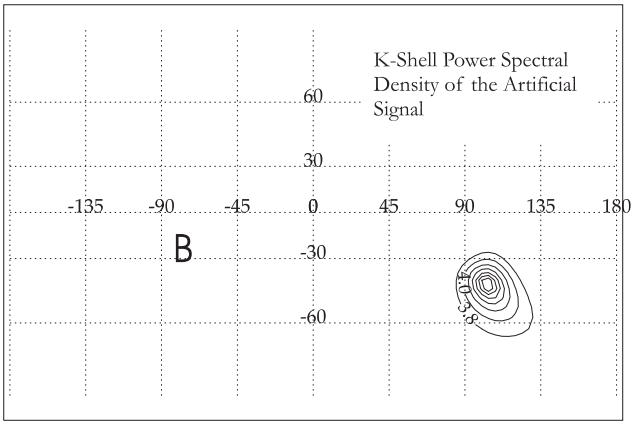

Fig. 3. Distribution of power on the k-shell $k = 0.0036\ \mathrm{km}^{-1}$ in a stereographic projection and logarithmic representation. B denotes the position of the mean magnetic field direction.

that the described wave telescope is a suitable tool to analyze multi-point magnetic field measurements with respect to any propagating wave and its wave vector.

3 A magnetosheath case study

To test the wave telescope with real data, we have chosen an interval at the beginning of the new millennium when the Cluster fleet cruised the far-Earth magnetosheath. Measurements from spacecraft Cluster 1 are displayed in Fig. 4. The spacecraft were approximately located at (9.3, 17.3, 2.3) R_E at a distance of $19.8\,R_E$, i.e. close to apogee. Large-amplitude transverse and compressional magnetosheath oscillations are dominating the observations. For a more detailed analysis, the interval 1 January 2001, 01:55–02:30 UT has been selected as it exhibits clear wave packets which will also allow for an analysis of wave propagation properties using a classical minimum variance analysis (e.g. Sonnerup

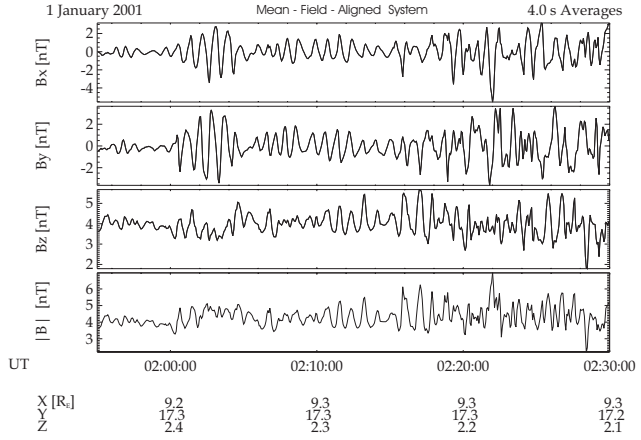

Fig. 4. Magnetic field observations recorded by Cluster 1 in the interval on 1 January 2001, 01:55–02:30 UT. The data are displayed in a mean field-aligned coordinate system with the B_Z direction aligned with the mean magnetic field direction.

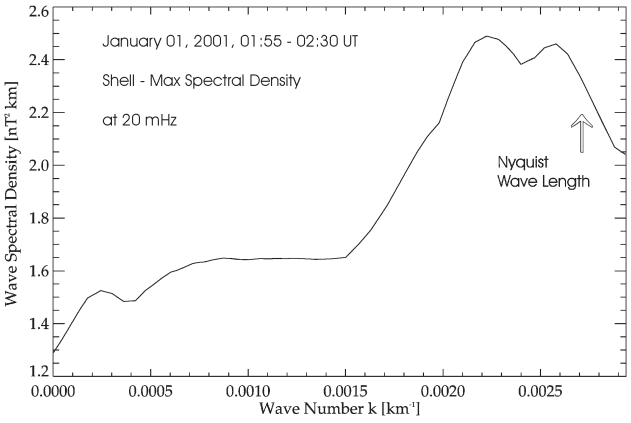

Fig. 5. Shell-max spatial spectral density distribution in logarithmic representation resulting from applying the wave telescope to measurements in the magnetosheath during the interval 1 January 2001, 01:55–02:30 UT.

and Cahill, 1967) and other means. A frequency spectral analysis exhibits a broad spectral power peak at (20±5) mHz. This frequency interval has been used to process the measurements with the wave telescope. 16 time intervals, each with a duration of 1024 s and shifted by 64 s have been Fourier analyzed to determine the averaged matrix $\mathcal{M}_B$ at a frequency of 20 mHz. The k-space was scanned with an angular resolution of 4° and a k-resolution of $5 \cdot 10^{-5}\,\mathrm{km}^{-1}$. The mean distance of the four spacecraft was 616 km. The Nyquist wave number, as defined above, is determined at $0.0027 \pm 0.0001\ \mathrm{km}^{-1}$, where the error estimate is based on taking into account the change in the Cluster configuration during the analysis interval. The configuration quality parameter was determined at $Q_{GM} = 2.24$, i.e. the configuration was not close to the ideal tetrahedron structure. The mean magnetic field vector in the analysis interval was (in spherical coordinates) (173°, −26°, 3.8 nT). In order to check for time stationarity and space homogeneity, we have computed the scattering of the mean magnetic field magnitude and direction surrounding this mean field, based on mean the field values determined for each spacecraft for the same intervals of 1024 s used for the k-analysis. The mean magnitude scatters by 0.12 nT, while the mean directions scatter by 3.8°. Thus we conclude that the data are stationary and homogeneous.

The result of the k-spectral analysis is displayed in Figs. 5 and 6. The spatial spectrum (not shown here) does not exhibit any clear spectral signature, but merely shows power decreasing with increasing k-value. The shell-max spatial spectral density distribution, however, exhibits a clear peak at $0.0022\,\mathrm{km}^{-1}$, corresponding to a wave length of 2856 km. A secondary peak at about $0.0026\,\mathrm{km}^{-1}$ is not discussed here any further, as this peak is very close to the Nyquist wave number.

As the observed waves are dominated by low-frequency compressional fluctuations, their dispersion relation may be

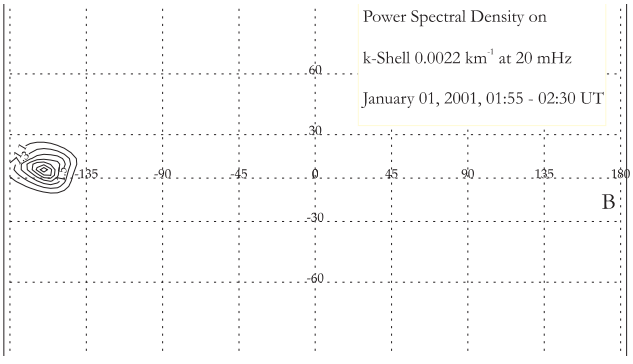

Fig. 6. Spectral density distribution on the k-shell $k = 0.0022\,\mathrm{km}^{-1}$ resulting from applying the wave telescope to measurements in the magnetosheath during the interval 1 January 2001, 01:55–02:30 UT. The logarithm of the power is displayed. 'B' denotes the position of the mean magnetic field direction.

approximated by the MHD fast mode relation $\omega/k = v_A$, where v_A is the local Alfvén phase velocity. With the above given values for $\omega = 2\pi f$ and the wave number k, we determine $v_A \approx 57$ km, a value reasonable for the terrestrial magnetosheath.

The spectral density distribution on the k-shell $k = 0.0022\,\mathrm{km}^{-1}$ is displayed in Fig. 6. A well focused spectral peak is located at (−160°, 6°), i.e. the wave telescope detected a rather narrow wave beam propagating almost in $-x$-direction. Wave propagation is off-angle at about 42° and is in an anti-parallel direction with respect to the ambient magnetic field vector. The mean velocity vector of the four spacecraft in the analyzed interval was (0.39, −0.13, −0.9) km/s, i.e. the spacecraft velocity was almost at a right angle with respect to the $\boldsymbol{k}$-vector. Thus, a Doppler shift due to spacecraft motion does not need to be taken into account.

To receive an independent determination of the wave propagation direction, the classical minimum variance technique

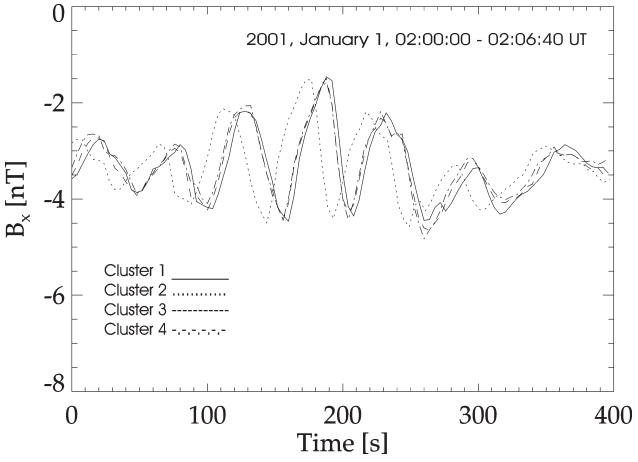

Fig. 7. Magnetic field measurements of the B_X component made at the four Cluster spacecraft in the time interval on 1 January 2001, 02:00–02:06 UT.

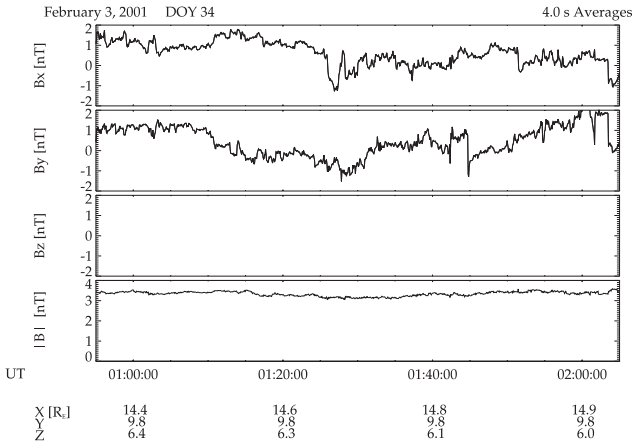

Fig. 8. Magnetic field measurements made on board the Cluster 1 spacecraft in the time interval 3 February 2001, 00:55–02:03 UT.

(e.g. Sonnerup and Cahill, 1967) has been applied to the measurements of all four spacecraft. The time interval analyzed was 1 January 2001, 02:00:00–02:05:15 UT. The derived eigenvalue ratios are $15.5 \pm 0.5 : 10.5 \pm 0.5 : 1$, averaged over all four spacecraft. The averaged minimum variance direction is given by $(-4.7°, 25.0°)$, corresponding to an angle of 175° between the mean magnetic field direction and the minimum variance direction, i.e. a classical minimum variance analysis almost provides one with field-aligned propagation direction if the minimum variance direction is interpreted as the propagation direction. Thus, the wave telescope analysis and the minimum variance analysis give slightly different results. A possible reason for this discrepancy is the selective nature of the wave telescope with respect to frequency and wave number. The minimum variance technique as applied here does not make any selection with respect to frequency and wave number.

To receive a further independent estimate for the wave propagation direction, we analyze in more detail measurements in the time domain. Figure 7 displays measurements of the B_X component made at all four spacecraft between 02:00:00 and 02:06:40 UT. Measurements made at Cluster spacecraft 1, 3, and 4 almost coincide, while the Cluster 2 spacecraft records the wave packet about 15 s earlier. We conclude that Cluster 1, 3, and 4 are located in the same phase plane. From the position vectors, the normal vector of the phase plane, $\boldsymbol{n}$, can be determined: $\boldsymbol{n} = (0.98, 0.22, 0.04)$. This normal phase plane vector determines a positive and a negative half space; the positive one is the one in the direction of $\boldsymbol{n}$. Introducing two half spaces allows one to introduce an oriented distance. The distance of the origin of the GSE-coordinate system to the phase plane is −82 213 km, i.e. the Earth lies in the negative half space with respect to the phase plane. The distance of Cluster 2 to this plane along the normal direction is 880 km, i.e. Cluster 2 lies in the positive half space. The angle of the Cluster 2 distance vector and the phase plane normal is calculated at 37.5°.

The mean spacecraft velocity vector is determined as $(0.39, -0.13, -0.9)$ km/s, from which an angle between the spacecraft velocity vector and the phase plane normal of 81° results, i.e. the configuration is moving almost perpendicular to the wave propagation direction. Thus, no Doppler effect needs to be taken into account.

As the signal is first detected at Cluster 2, it propagates from this spacecraft towards the other three, thus defining the phase plane. As the distance of Cluster 2 with respect to this plane is positive, the wave must propagate in a direction anti-parallel to the normal $\boldsymbol{n}$, i.e. the unit $\boldsymbol{k}$-vector is given by $\boldsymbol{e}_k = -\boldsymbol{n} = (-0.98, -0.22, -0.04)$, from which a wave propagation in the direction $(-167.3°, -2.3°)$ results. This is almost identical to the wave propagation direction determined using the wave telescope technique.

The wave length and wave number can be determined from the distance between the Cluster 2 spacecraft to the phase plane as well as the delay time of the signal's arrival at the spacecraft. With a wave period of 50 s and an advanced arrival time of 15 s, a phase difference of 108° at a distance of 880 km results. From this, the wave length is determined at $(2\,933 \pm 263)$ km, where the error estimate is based on assumption of an uncertainty in the wave period of ±5 s. Thus, both wave propagation direction as well as wave length coincide very well with those values determined using the wave telescope. This qualifies our new analysis technique.

4 A Solar wind case study

To further test the wave telescope, we have chosen an interval when the spacecraft cruised the near-Earth solar wind at about (14.6, 9.8, 6.3) R_E at a distance of about 18.7 R_E. The ambient magnetic field is dominated by about a 3.5 nT Z-component (see Fig. 8), i.e. a northward pointing interplanetary magnetic field. In order to check for time stationarity and space homoneity, we have computed the scattering of the mean magnetic field magnitude and direction surrounding

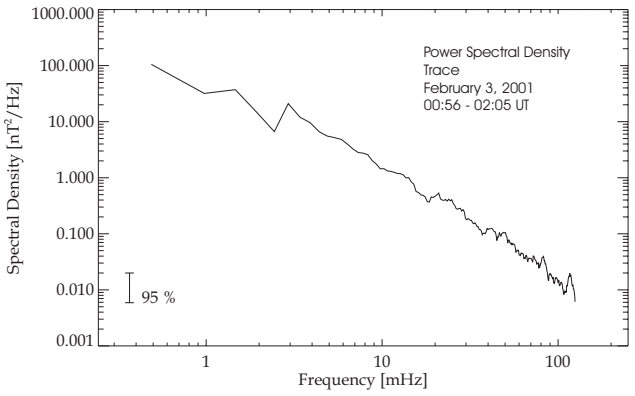

Fig. 9. Trace of the frequency power spectral density matrix determined using data displayed in Fig. 8.

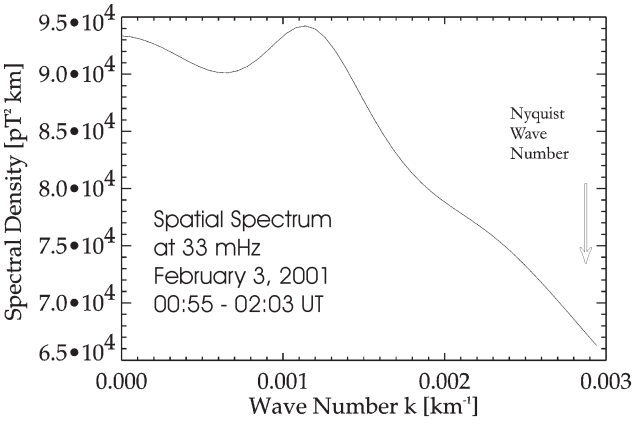

Fig. 10. Spatial spectrum determined using magnetic field data from all four Cluster spacecraft in the interval on 3 February 2001, 00:55–02:03 UT. The logarithm of the power is displayed.

this mean field based on the mean field values determined for each spacecraft for the same intervals of 1024 s used for the k-analysis. The mean magnitude scatters by 0.12 nT, while the mean directions scatter by 2.8°. Thus, we conclude that the data are stationary and homogeneous.

Small-amplitude transverse oscillations are dominating with the compressional component exhibiting only minor fluctuations, i.e. the oscillations are transverse or Alfvénic in nature. A frequency spectral analysis does not reveal any power spectral peak (see Fig. 9), but in the frequency range (0,125) mHz, the spectrum is rather featureless with a spectral index of about -2.

For a more detailed analysis the interval 3 February 2001, 00:55–02:03 UT has been selected. The mean distance between the spacecraft was 576 km. The Nyquist wave number was determined at $k_{\rm NY} = 0.0029 \pm 0.0001\,{\rm km}^{-1}$. The configuration quality parameter was determined at $Q_{GM} = 2.33$. The mean magnetic field vector is (35°, 76°, 3.15 nT), and the spacecraft were moving almost in the X-direction with velocity 1.2 km/s at an angle of 72° to the mean magnetic field direction.

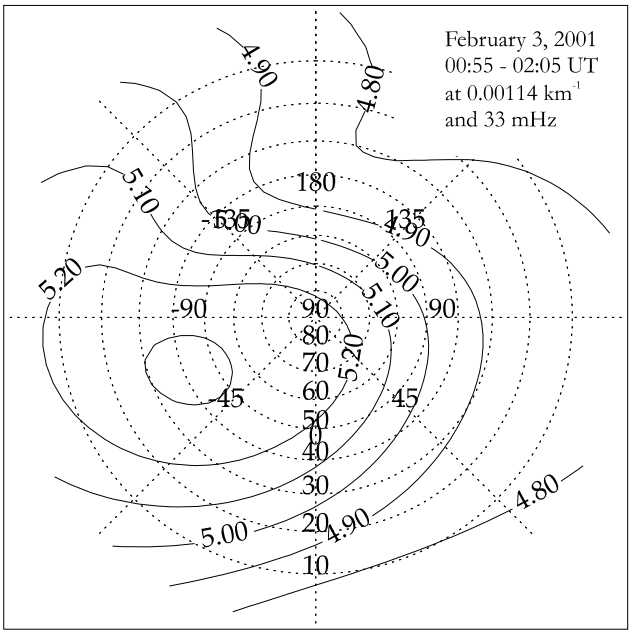

Fig. 11. Spectral density distribution on the k-shell $k = 0.00115\,{\rm km}^{-1}$ resulting from applying the wave telescope to measurements in the solar wind during the interval on 3 February 2001, 00:55–02:05 UT. The logarithm of the power, given in pT, is displayed.

The k-space of this interval has been scanned at various frequencies since no clear frequency spectral peak is detected. The scanning parameters are as before. In the frequency interval 30–36 mHz, the spatial spectral density distribution exhibits a clear peak at $k = 0.00114\,{\rm km}^{-1}$, i.e. at a wave length of 5511 km (Fig. 10). One should remember that the spatial k-spectrum has been determined by averaging all the power at a given k over longitude and latitude. In the magnetosheath case study, this distribution does not exhibit any clear peak, while the shell-max spectrum does. The reason for this was that the averaging procedure smeared out any spectral peak. Now in the present case, a peak already in the spatial spectrum indicates a rather broad spectral distribution. This is demonstrated in Fig. 11, where the power distribution in a stereographic representation is displayed. The power distribution is rather broad with a shallow maximum at about (67°, 42°).

As in the magnetosheath case, we can estimate the phase velocity using the known values of ω and k. For an Alfvénic-type low frequency fluctuation we expect a dispersion relation

$$\frac{\omega}{k} = v_A \cos\theta, \tag{19}$$

where θ denotes the angle of propagation with respect to the ambient magnetic field. With a mean angle of propagation of 53°, the Alfvén velocity is determined at 302 km/s, a value much too high for typical solar wind conditions, but comparable to the solar wind flow velocity itself. This indicates that

the solar wind associated Doppler effect needs to be taken into account. A more proper dispersion relation is given by

$$\omega = \boldsymbol{v}_A \cdot \boldsymbol{k} + \boldsymbol{v}_{SW} \cdot \boldsymbol{k}, \quad (20)$$

where $\boldsymbol{v}_A$ denotes the vector Alfvén velocity and v_{SW} is the solar wind flow velocity vector. With $\boldsymbol{k} = (33, 78, 76) \cdot 10^{-5}\,\mathrm{km}^{-1}$, and $\boldsymbol{v}_A = v_A \cdot \boldsymbol{e}_B$, where $\boldsymbol{e}_B = (0.20, 0.14, 0.97)$ is the unit vector of the mean solar wind magnetic field, and by approximating $v_{SW} = (-400, 0, 0)$ km/s, Eq. (20) allows one to determine the Alfvén velocity required to fulfill the Doppler shifted dispersion relation: $v_A \approx 83$ km/s, which is a reasonable value.

The difference between the magnetosheath case, where only the shell-max spectrum revealed the wave beam, and the present case may be understood in the following way. For compressional fast mode type low-frequency waves, the MHD dispersion relation requires

$$\frac{\omega}{k} = v_A, \quad (21)$$

i.e. for any given ω, only one k is allowed. Thus, a small variation in frequency causes a change in the k-value with the effect that this wave no longer contributes to the power of that k-shell analysed. A narrow wave beam is thus expected for fast mode type waves.

The width of the frequency spectral distribution, $\delta\omega$, is related to that of the k-distribution, δk, via

$$\frac{\delta\omega}{\delta k} = v_A. \quad (22)$$

In the magnetosheath case, $\delta\omega \approx 31.5$ mHz, correspondes to an uncertainty $\delta k \approx 0.0006\,\mathrm{km}^{-1}$, which fits the observations.

In the solar wind case discussed, we have one more degree of freedom to fulfill the dispersion relation: the propagation angle. Variations in both k and θ need to be taken into account when interpreting the spatial spectrum and the shell-max spectrum. Assuming $k = \text{const}$, any variation in ω is related to a change in the propagation direction via

$$\frac{\delta\omega}{\delta(\cos\theta)} = v_A\, k. \quad (23)$$

With $v_A = 83$ km/s, $k = 0.00114\,\mathrm{km}^{-1}$, and $\delta\omega = 37.7$ mHz, which is a value resulting from the frequency range in which the discussed wave has been detected, we have $\delta(\cos\theta) \approx 0.4$. Such a large possible scattering in θ may explain the broad spatial spectral power distribution shown in Fig. 11.

5 Summary and outlook

We have successfully demonstrated the capabilities of the wave telescope technique for the first time and applied it to magnetic field measurements from the four Cluster spacecraft. In the outer magnetosheath, large-amplitude transverse and compressional fluctuations propagating in an anti-solar direction with a wave length of about 2900 km have been detected. In the near-Earth solar wind, an Alfvénic type perturbation has been analyzed, propagating almost along the positive Y-axis towards the southern hemisphere at a wave length of about 5500 km.

The wave telescope proves to be a very valuable tool in the analysis of low-frequency waves in a space plasma. Here, we do not attempt any physical interpretation, but merely wish to demonstrate the capability of the new tool. It generates vast amounts of new information, i.e. a power distribution $P(\omega, \boldsymbol{k})$, which requires new ways of graphical interpretation. The spatial spectrum density distribution $P(\boldsymbol{k})$ has been introduced by averaging the power on any given k-shell. This spectrum does not give any resolution in direction, but merely in wave number. To display wave beams, i.e. those waves exhibiting a very localized power distribution on a given k-shell, the shell-max spectrum has been introduced. Angular resolution is gained when selecting that k-shell which exhibits maximum power in a shell-max spectrum and then displaying the power distribution on the maximum k-shell.

The problem of spatial aliasing has been solved in a conservative form, i.e. the Nyquist wave number has been determined as the radius of the k-sphere, that is the sphere that can be inscribed into the k-cell, whose determination has been outlined above. This wave number defines that part of the k-space where the analysis is done. Future work will be done by taking into account the full k-cell.

The wave telescope method itself has been tested against a classical minimum variance technique applied separately to all four spacecraft. Both analysis tools give somewhat different results, for reasons that are not entirely clear, but probably attributable to the fact that the wave telescope is selective in ω and k. To further validate the new tool, we did a case study where three of the spacecraft were lying almost on the same wave phase plane, while the fourth one was detached from this plane. A wave number and wave direction determination using this special situation gives one results consistent with the wave telescope tool.

Future work will concentrate on a systematic study of the magnetosheath and near-Earth wave propagation characteristics, as well as the combining of the wave telescope tool with the mode decomposition technique, as introduced by Glassmeier et al. (1995) and Vocks et al. (1999). This mode decomposition technique is similar to the pure state analysis introduced by Samson and Olsen (1980) and Samson (1983), but using, for example, MHD eigenvectors as prescribed state vectors. Determination of these eigenvectors requires knowledge about the wave propagation direction, which is obtainable from the wave telescope.

We conclude that this first study of Cluster magnetometer measurements using the wave telescope technique gives one extremely promising first results. However, the new tool also has its weak points as it can only be applied to longer intervals of observations which guarantee time stationarity and spatial homogeneity. Furthermore, the spacecraft configuration should not change too much over the analysis interval. In

addition, as already mentioned, a lot of new spectral information is generated, which needs to be evaluated and requires future and more detailed studies on the confidence levels of the estimators used. Combining spatial and temporal spectral information requires more detailed studies on Doppler effects, i.e. in addition to magnetic field information flow, velocity measurements are also important.

Acknowledgements. Cluster is a joint ESA/NASA spacecraft mission. The work at the Technical University of Braunschweig is financially supported by the Deutsches Zentrum für Luft- und Raumfahrt DLR and the German Bundesministerium für Bildung und Wissenschaft under contract 50OC0103. We are especially grateful to the Cluster Project Scientists Rudi Schmidt and Philippe Escoubet and the Project Manager John Ellwood and all their colleagues at ESA, who made this mission a real step into a new millenium of magnetospheric physics.

Topical Editor M. Lester thanks two referees for their help in evaluating this paper.

References

Balogh, A., et al.: The Cluster Magnetic Field Investigation, in: The Cluster and Phoenix Missions, (Eds) Escoubet, C. P., Russell, C. T., and Schmidt, R., Kluwer Academic Publishers, Dordrecht, 1997.

Capon, J., Greenfield, R. J., and Kolker, R. J.: Multidimensional maximum-likelihood processing of a large aperture seismic array, Proc. IEEE, 55, 192–213, 1967.

Chanteur, G.: Spatial interpolation for four spacecraft: Theory, in: Analysis methods for multi-spacecraft data, (Eds) Paschmann, G. and Daly, P. W., ISSI Sci. Rep. SR-001, pp. 349–369, Bern, 1998.

Dunlop, M. W., Southwood, D. J., Glassmeier, K. H., and Neubauer, F. M.: Analysis of multipoint magnetometer data, Adv. Space Res., 8, 273–277, 1988.

Dunlop, M. W., Woodward, T. I., Southwood, D. J., Glassmeier, K. H., and Elphic, R.: Merging 4-spacecraft data: Concepts used for analysing discontinuities, Adv. Space Res., 20, 1101–1106, 1997.

Dunlop, M. W. and Woodward, T.: Analysis of thick, non-planar boundaries using the discontiuity analyser, Ann. Geophysicae, 17, 984–995, 1999.

Glassmeier, K. H., Motschmann, U., and Schmidt, R., (Eds) in: Proceedings of the CLUSTER Workshop on Data Analysis Tools, ESA SP-371, Noordwijk, 1995.

Glassmeier, K. H., Motschmann, U., and v. Stein, R.: Mode recognition of MHD wave fields at incomplete dispersion measurements, Ann. Geophysicae, 13, 76–83, 1995.

Harjes, H. P. and Henger, M.: Array-Seismologie, Z. Geophysik, 39, 865–905, 1973.

Kittel, Ch.: Einführung in die Festkörperphysik, München, 1973.

Motschmann, U., Woodward, T. I., Glassmeier, K. H., and Dunlop, M. W.: Array Signal Processing Techniques, Proc. CLUSTER Workshop on Data Analysis Tools, (Eds) Glassmeier, K. H., Motschmann, U., and Schmidt, R., ESA SP-371, Paris, pp. 79–86, 1995.

Motschmann, U., Woodward, T. I., Glassmeier, K. H., Southwood, D. J., and Pinçon, J. L.: Wavelength and direction filtering by magnetic measurements at satellite arrays: Generalized minimum variance analysis, J. Geophys. Res., 101, 4961–4965, 1996.

Motschmann, U., Glassmeier, K. H., and Pinçon, J. L.: Multi-spacecraft filtering: Plasma mode recognition, in: Analysis methods for multi-spacecraft data, (Eds) Paschmann, G. and Daly, P. W., ISSI Sci. Rep. SR-001, Bern, pp. 79–89, 1998.

Musmann, G., Beinroth, H. J., Denskat, U., Hente, B., Theile, B., and Neubauer, F. M.: Proposal for a Plasma Wave Array Experiment to be Flown on the ESA Spacelab, Proposal submitted to the European Space Agency, Braunschweig, May 1974.

Neubauer, F. M. and Glassmeier, K. H.: Use of an array of satellites as a wave telescope, J. Geophys. Res., 95, 19 004–19 011, 1990.

Paschmann, G. and Daly, P., (Eds) in: Analysis methods for multi-spacecraft data, ISSI Scientific Report, SR-001, Bern, 1999.

Pinçon, J. L. and Lefeuvre, F.: Local characterization of homogeneous turbulence in a space plasma from simultaneous measurement of field components at several points in space, J. Geophys. Res., 96, 1789–1802, 1991.

Pinçon, J. L. and Lefeuvre, F.: The application of the generalized Capon method to the analysis of a turbulent field in space plasma: Experimental constraints, J. Atmos. Terr. Phys., 54, 1237–1247, 1992.

Pinçon, J. L.: Cluster and the k-filtering, Proc. CLUSTER Workshop on Data Analysis Tools, (Eds) Glassmeier, K. H., Motschmann, U., and Schmidt, R., ESA SP-371, Paris, pp. 87–94, 1995.

Pinçon, J. L. and Motschmann, U.: Multi-Spacecraft Filtering: General Framework, in: Analysis methods for multi-spacecraft data, (Eds) Paschmann, G. and Daly, P. W., ISSI Sci. Rep. SR-001, pp. 65–78, Bern, 1998.

Robert P., Roux, A., Harvey, C. C., Dunlop, M., Daly, P. D., and Glassmeier, K. H.: Tetrahedron geometric fatcors, in: Analysis methods for multi-spacecraft data, (Eds) Paschmann, G. and Daly, P. W., ISSI Sci. Rep. SR-001, Bern, pp. 323–348, 1998.

Samson, J. C. and Olson, J. V.: Some comments on the descriptions of polarization states of waves, Geophys. J.R. Astron. Soc., 61, 115–129, 1980.

Samson, J. C.: Pure states, polarized waves, and principal components in the spectra of multiple, geophysical time-series, Geophys. J. R. Astron. Soc., 72, 647–664, 1983.

Sonnerup, B. U. Ö. and Cahill, L. J.: Magnetopause structure and attitude from Explorer 12 observations, J. Geophys. Res., 72, 171–183, 1967.

Stein, vom, R., Glassmeier, K. H., and Dunlop, M.: A configuration parameter for the Cluster satellites, Technical Report No. 2/92, Inst. f. Geophysics, Technical University of Braunschweig, Braunschweig, 1992.

Stein, vom, R., Glassmeier, K. H., and Motschmann, U.: CLUSTER as a Wave Telescope and Mode Filter, Proc. Workshop on the Spatio-Temporal Analysis for Resolving Plasma Turbulence, ESA WPP-47, Paris, 1993.

Vocks, C., Motschmann, U., and Glassmeier, K. H.: A mode filter for plasma waves in the Hall-MHD approximation, Ann. Geophysicae, 17, 712–722, 1999.